PROCEEDINGS REPRINT

SPIE–The International Society for Optical Engineering

Reprinted from

Characterization, Propagation, and Simulation of Sources and Backgrounds III

12–13 April 1993
Orlando, Florida

Volume 1967

Measured and simulated power spectral density and temporal coherence of infrared cirrus and stratus cloud images

Morton Farber, Jerry Tessendorf, Albert Soong

Areté Associates, P.O. Box 6024, Sherman Oaks, CA 91413

ABSTRACT

Sets of image data from the MUSIC (Multi Spectral Infrared Camera) have been analyzed to obtain the spatial and temporal structure of cirrus and stratus cloud scenes at small spatial and temporal scales. The MUSIC data were collected in 1989 in a side-looking airborne geometry. The large clutter to noise ratios found in this analysis for both cirrus and stratus clouds represent a potentially large noise source for IRST. The power-law roll-off and anisotropy of the power spectral density of images is compared to the output of a 3-D cloud scene simulator and found to be in reasonable agreement; and in very poor agreement with simpler notions which invoke perspective distortion of two-dimensional clouds and predict much large anisotropy. The log of the time-lagged coherence of a registered sequence of images depends on the square of the spatial frequency and the square of the time lag. This is in agreement with a passive advection model of the cloud evolution, which successfully predicts the change in coherence behavior between smaller and large time lags relative to the advection integral time.

1. INTRODUCTION

A key consideration in the design and operation of an airborne IRST (Infrared Search and Track) system is the spatial and temporal structure of the cloud clutter backgrounds. For a wide variety of scenes and sensor configurations, the measured noise in the output radiance field due to the scene background is far higher than the sensor related noise (BLIP, readout, etc.). It is, therefore, important to be able to characterize measured scenes in a way that directly relates to target measurements. For this reason we have chosen to measure the 2-D power spectral density (PSD) of the scene along with the temporal coherence. We have used this parameterization in a previous study of backgrounds due to cumulus clouds, as measured by the IRAMMP sensor.[1]

For the present study, we analyze the spatial/temporal structure of cirrus and stratus cloud scenes. The data were collected using the MUSIC (Multi Spectral Infrared Camera) sensor mounted side looking on a Canberra aircraft. Data collected by the sensor for other applications have been analyzed and reported elsewhere.[2,3] The sensor consists of a 45 x 90 staring array with an IFOV of 500 μrad. There are dual focal planes for collecting data in both LW and MW bands along with a series of narrow band filters. The NEΔT for the data discussed here is 0.08K. It has a framing rate of 80 Hz which makes the data especially useful for measuring temporal coherence. Cloud measurements made using the MUSIC offer a unique opportunity to characterize the IR radiance field at relatively small (on the order of a few meters) spatial scales. This can be contrasted with power spectra measurements derived from satellite-based sensors in which spatial resolution elements are on the order of hundreds of meters.[4,5] In addition to the small spatial scales that are resolvable using the MUSIC sensor, the low grazing angle geometry is unique relative to ground-based or satellite-based observations.

While empirical characterization of clutter backgrounds is an important step in understanding and dealing with those backgrounds, it is often necessary to be able to predict and model a wide variety of clutter backgrounds. To this end, Areté has developed a 3-D cloud simulation model in which, with a few key parameters to describe the mean and fluctuation statistics of the temperature and condensed water content in the cloud field, the radiance at the focal plane in the LW band can be derived. The simulated radiance from the cloud field is calculated by computing the radiative transport along sets of rays. In the present analysis, we have compared the PSD predictions from the simulated outputs to the MUSIC measurements, using a range of cloud parameters consistent with in-situ cloud measurements. From this analysis, we can extract the key cloud parameters that determine measured cloud clutter levels.

In the following section of this paper we describe the selected MUSIC scenes and geometries in greater detail. The measured spatial power spectra and the measured temporal coherence are examined for the cirrus and stratus data in Section 3. Predictions from the Areté 3-D cloud simulator, along with a description of the model are given in Section 4. In particular, we discuss the anisotropic characteristics of the PSDs expected at low grazing angles. In this section, we also discuss a model for temporal coherence within clouds and comparisons with measured coherence functions. Finally in Section 5, we present the

0-8194-1203-1/93/$6.00

summary and conclusions of this analysis.

SECTION 2. SCENE SELECTION AND DATA PROCESSING

The data used in the analysis was collected over the Oregon coast in 1989. All the measurements to be discussed here were obtained with a bandpass of 8.43 - 8.91 μm. Before the data could be used to extract the spatial and temporal spectra, calibration and sensor artifact removal had to be carried out. The steps in this process for a selected set of frames are shown in Figures 1a - 1d. The raw data are shown in Figure 1a. Cloud imagery is not readily apparent at this initial stage. To process these data, we first interpolate over regions or columns which are known to be bad (Figure 1b). The data are then calibrated with a 2 point linear calibration using inflight blackbody calibration measurements (Figure 1c). In this step A/D counts are converted to spectral radiance. After the data are calibrated, tests are done to interpolate over pixels that are flagged as outliers. This is done by first identifying pixels that are more than 10 standard deviations from the scene mean. After these extremely bad pixels (stuck A/D bit, etc.) are removed, tests are made in local regions, typically 8 x 8 pixel regions, to identify pixels that are four standard deviations away from the local mean. The tested region is slid across the focal plane so that all pixels are examined.

At this point in the processing, the data have been calibrated and bad pixels have been removed. We find the image at this point contains a strong pattern noise component which manifests itself as pixel-to-pixel random fluctuation in the measurements. This is due largely to uncalibrated, non-linear response variations between pixels. To suppress the pattern noise the scene is temporally demeaned on a pixel-by-pixel basis using an extended superset (typically about 30 seconds) of the data under study. This correction is based on the idea that each pixel sees the same average scene content over a relatively long time period. The mean of the entire scene is added back to preserve the measured radiance levels. As a final filter to remove the pattern noise, we Fourier transform each frame using a FFT, and remove that portion of the 2-D PSD corresponding to both k_{AZ} and $k_{El} > ½$ Nyquist jointly. This is based on the physically reasonable assumption that there is relatively little true scene content relative to noise, at these spatial frequencies. At this point (Figure 1d), high quality cloud imagery is apparent.

Table 1. Selected MUSIC Scenes
Band: 8.43 to 8.91 μm

Scene	Platform Alt (km)	Cloud Alt (km)	Range (km)	Aspect (0)	Cloud Temp °C	Comment
4-1	8.2	9.4	43	0-1	-38	Bands of cirrus
4-2	8.2	9.4	33	2	-38	Bands of cirrus
5-2	8.8	8.8	20	Side	-29	Thin cirrus
5-3	8.8	8.8	11	Side	-29	Thin cirrus
5-4	8.8	8.8	11	Side	-29	Thin cirrus
6-1	2.1	2.0	19	0-2	8	Stratus bed with 1 *k* ft. ledge
6-2	2.1	2.0	9	0-2	8	Stratus bed with 1 *k* ft. ledge
6-3	5.5	2.0	11	18	8	Stratus bed with 1 *k* ft. ledge
6-4	8.8	2.1	20	20	8	Stratus bed with 1 *k* ft. ledge
6-5	8.8	2.1	20	20	8	Stratus bed with 1 *k* ft. ledge
6-6	8.8	2.1	20	20	8	Stratus bed with 1 *k* ft. ledge

The pre-processing described above was applied to a set of MUSIC scenes containing cirrus and stratus clouds. The key scene characteristics are summarized in Table 1. Many of the measurements were made at side aspects or at low grazing

angles. The pre-processed imagery for representative sets of cirrus and stratus scenes are shown in Figure 2 and Figure 3. It should be kept in mind that the gray scale imagery is self normalized so that dark areas do not imply "blue" sky regions. Indeed, measured temperature variations are no more than a few degrees. An interesting feature of the cirrus imagery is the smoothed and horizontally stretched appearance. As we will discuss further in the following sections, this is a consequence of the elongated footprint due to the very low grazing angles.

SECTION 3. SPATIAL AND TEMPORAL ANALYSIS OF SCENES

In order to analyze the spatial structure of the cloud scenes and to compare with simulation predictions, the 2-D power spectra of the scenes were obtained. A representative cirrus scene and its spectrum is shown in Figure 4, and for a stratus scene in Figure 5. In the lower right portion of each figure, we show the 2-D PSD as a contour plot (5 dB contours) while on the left we have plotted the azimuthal and elevation cuts from the 2-D PSD. The spatial frequency axis is in units of cycles/meter where the Nyquist frequency is set by the nominal range and IFOV. For the azimuthal cuts we see that after a breakpoint corresponding to several hundred meters to ~ 1 km in physical distance there is a power low roll-off. In these scenes the clutter drops to the systems noise level at high spatial frequencies. A similar behavior is seen for the elevation cuts but with breakpoints shifted to larger spatial frequencies and with larger values of the power spectra at a given frequency. This behavior is qualitatively what we would expect because of the foreshortening at the very low grazing angles. However, as we will discuss

Table 2. Spatial Characteristics of Measured Stratus and Cirrus Scenes

Case	Range (km)	CNR (dB)	Clutter Spectrum Roll-off AZ	Clutter Spectrum Roll-off El	CNR (dB) *40 km	Ratio of Elevation to Azimuthal Clutter (dB)
CIRRUS SCENES						
4-1	40.0	31.4	-4.6	-6.3	31.4	16.7
4-2	10.0	17.9	-4.1	-6.4	34.9	3.1
5-2a	20.0	32.9	-5.5	-4.6	42.1	20.2
5-2b	20.0	23.2	-6.6	-2.8	32.4	12.5
5-3	10.0	19.3	-6.2	-4.2	36.3	5.0
5-4	10.0	18.0	-4.7	-4.7	35.0	4.6
STRATUS SCENES						
6-1	20.0	15.5	-3.9	-4.6	22.7	2.1
6-2	10.0	19.3	-4.8	-4.8	33.8	14.4
6-3	10.0	13.9	-4.2	-3.9	28.4	2.4
6-4	20.0	26.2	-4.4	-4.6	33.4	2.3
6-5	20.0	28.5	-4.6	-4.8	35.7	10.8
6-6	20.0	28.8	-4.3	-6.1	36.0	8.1

* CNR at 40 km based on power law $P \sim k^{-m}$ with m = 5 for cirrus and m = 4.5 for stratus.

again shortly, the relative spectral power in the elevation and azimuthal deviations cannot be quantitatively explained on the

basis of an opaque 2-dimension cloud model. The measured spectra for the stratus clouds are observed to be qualitatively quite similar to cirrus behavior.

The measured spectral roll-off rates in the azimuthal and elevation directions assuming a power law dependence $P \sim k^{-m}$, are given in Table 2 for the measured MUSIC scenes. To obtain the decay rates shown in the table, a least squares fit is done using the azimuthal and elevation cuts (see Figures 4 and 5). In performing the fits, the plateau regions at low k values are excluded. On the high k end, data that are significantly rolled off by the MUSIC system transfer function (shown in the figures) are not included. It is also required that the clutter spectral levels be at least 10 dB above estimated system noise levels. Measured roll off rates are typically about -5 ± 1.5 for the cirrus measurements and comparable for both the azimuthal and elevation cuts. In the stratus scenes the rates are somewhat lower, typically about -4.5 ± 0.5. These rates should be compared with predictions of a 3-D turbulence model in the limit of high spatial frequencies where the decay rate of -11/3 is to be expected.[6] The more rapid decay rates in the measured radiance field are likely the results of large fluctuations in the transmission properties along various lines of sight within the cloud. This, in turn, gives rise to high order non-linear effects which in effect convolve power spectra and cause more rapid roll-off. The larger decay rates observed for cirrus clouds may, therefore, be a result of the large fluctuation in optical properties associated with the cirrus formations.

In addition to the spectral decay rates, the observed clutter-to-sensor noise ratios for the measured scenes are tabulated. In order to compare the scenes with each other we have also scaled the measurements to the arbitrary range of 40 km. This scaling has been done assuming a power law roll-off in the spectral levels; the assumption is that the minimum observable spatial frequency k_{min} is inversely proportional to the range. We also corrected for effects of transmissivity on clutter, as determined from LOWTRAN 7 using the mid latitude summer model. The large CNR values given in the table indicate that cirrus and stratus cloud backgrounds represent a potentially large noise source for an IRST. The measured cirrus scenes typically have somewhat greater clutter levels (a few dB) than the stratus scenes. This, again, is a result of the larger variation in optical properties across the cirrus cloud fields.

A significant feature of both the imagery and the PSDs is the obvious asymetry between the elevation and azimuthal directions. The anisotropy measurements are summarized in Table 2. These values were obtained by calculating the average variance along the azimuthal and elevation directions and taking the ratio of elevation to azimuthal variance. The measured anisotropy is observed to be highly variable and similar for both cirrus and stratus clouds; values are typically 2-15 dB. These values, however, should be compared with predictions from a purely geometic foreshortening model in which the cloud is modeled as an opaque 2-dimensional flat, blackbody emitter. In that case, for a power law PSD, it is straightforward to show that the elevation to azimuthal ratio, r, should be given by:

$$r = (\cos\theta)^{1-m} \tag{1}$$

If we substitute into the above equation $\theta = 88°$ or $2°$ grazing angle with respect to the flat cloud bottom, and $m = 5$, we would get a value r for 58 dB. This ratio is obviously far larger than the values given in Table 3, and clearly suggests that 3-dimensional effects, due to the finite optical depths in clouds as well as non-power law behavior, play a significant role, consistant with the predictions of the 3-D simulator. The modeling of the effects is discussed in Reference 7.

We next turn our attention to the temporal coherence of the measured scenes. In order to perform this analysis, however, it is first necessary to align or register the set of frames. To do the registration, we made use of a registration technique previously developed at Areté and described in Reference 1. The essential element in the "rubber sheeting" approach consists of dividing the scene into a set of small overlapped patches. Using a chi-squared metric consisting of the sums of squares of the difference in radiance between data in two frames, a given patch of data in one frame is shifted with respect to data in a second frame so as to minimize the metric. Sub-pixel registration accuracy is achieved by interpolation of the chi-squared surface. To analyze a MUSIC scene, a set of approximately 100 frames were registered together using the middle frame as the reference frame. From the curvature of the chi-squared surface for three ensembles of patches, we have estimated the registration accuracy (Cramer-Rao Bound). Registration accuracy in the azimuthal direction has been estimated at ~ .1 pixel for scenes with lower CNR values. In the elevation direction, the larger clutter values yield estimated registration accuracies of .05 pixels or less. These levels of registration error lead to loss in coherence which is negligible compared to measured losses except at very short times and at spatial frequencies near Nyquist.

The coherence for a set of frames is found by taking the 2-D FFT of each frame in the set. The coherence corresponding to a given temporal lag is found by forming the ensemble spectra and cross spectra for pairs of frame with the given lag (see also Reference 1). Slices from the coherence surface can then be plotted as a function of k or t and errors based on statistical uncertainties related to the number of degrees of freedom associated with a given coherence estimate can be found using standard techniques.[8] Slices of the coherence surface are shown in Figure 6 for a sample cirrus scene. The log coherence values are plotted in the figure as both a linear and quadratic function of k and t. Clearly the data are much better fitted by a quadratic dependence for both k and t. Stratus scenes exhibited similar behavior as shown by the example in Figure 7.

As we will see in the next section, for short time lags (less than a few seconds), the temporal decorrelation can be modeled as

$$\gamma^2(k,t) = \exp\,[-\sigma_v^2\, k^2\, t^2] \tag{2}$$

where k is spatial frequency in radians/meter and σ_v (m/sec) is the apparent turbulent velocity in the scene. By fitting various cuts in the coherence surface for several scenes, we find that typical values for σ_v range from approximately 11 m/sec to 23 m/sec. Since these values are far higher than levels associated with intrinsic turbulent motion within a stratus or cirrus cloud (~ 1 m/sec or less), we interpret these results as evidence that the measured temporal decorrelation is driven mainly by parallax-induced effects. This effect arises because of the finite optical penetration depth within a cloud and is discussed further in the next section.

SECTION 4. CLOUD MODELING AND PREDICTIONS

An important goal of this data analysis is to obtain a better understanding of the connection between cloud microphysics and the PSDs of images. Toward this goal, Areté has developed a cloud scene simulator which generates cloud realizations based on microphysical and statistical models, and images them as described briefly in Section 4.1. The resulting images of simulated clouds can then be subjected to PSD analysis in identical fashion as the MUSIC data. Because there is no cloud truth data in the MUSIC database, we have generated several simulated scenes with microphysics that span the likely range of realizable environmental conditions. In Section 4.2 the set of simulated scenes are described, along with the results of PSD analyses and comparisons to the MUSIC results.

To better understand the behavior of the temporal coherence, we have developed a model based on the passive advection of cloud structures, with a stochastic velocity field that decorrelates over time and space. Under relatively general circumstances, the $k^2 t^2$ behavior noted in Section 3 is predicted at "short" time separations, and at "long" time scales the $k^2 t$ behavior noted previously in IRAMMP data is also predicted. The terms "short" and "long" are defined in terms of the integral time scale of the stochastic advection velocity. These model predictions are presented in detail in Section 4.3.

4.1 Cloud Scene Simulator

The cloud scene simulator developed by Areté Associates attempts to model longwave infrared images of three-dimensional clouds, using cloud microphysical parameters to generate three-dimensional realizations of clouds, and radiative transfer theory to calculate their emitted radiance at the sensor. The simulator has been described in detail elsewhere,[7,9] and so is only outlined here. The simulator employs a three-step process. In the first step the simulator generates a three-dimensional cloud based on user-specified statistical characteristics for the mean, variance, and power law of the fluctuations of condensed water content and temperature. The second step converts these three-dimensional realizations of condensed water and temperature into optical properties — specifically the local blackbody radiance and the absorption coefficient. Images are generated in the third step, using a ray trace procedure to burrow through the cloud and accumulate properly-attenuated blackbody emissions. For the cirrus and stratus simulations reported below, the important variable quantity is the condensed water content.

Previous analyses of the cloud simulator output images have shown that at low grazing angles the PSD of the cloud is highly anisotropic, but not to the degree that would be predicted if the cloud radiance were emitted only from a thin quasi-two-dimensional region near the surface. The three-dimensional structure of the clouds is very important to the formation

of the PSD at any viewing angle. By the same measure, the MUSIC PSD analysis in Section 3 supports this view, since the anisotropy of those PSDs is less than expected for an opaque two-dimensional cloud by several orders of magnitude.

4.2 Cirrus Simulations

The cirrus simulations conducted for this analysis used the MUSIC 4-1 geometry as a baseline, and were created for several different profiles of the condensed water mean and variance. The same random number seed was used for each of the realizations of fluctuations. The camera was at a distance of 42.6 km from the front face of the cloud, looking up at the face at an angle of 1.75 degrees. Four realizations were generated using the water content values shown in Table 3. The images are shown in Figures 8 and 9. Visually, the character of the clutter in the four simulations is remarkably varied, with clutter variance levels from 12 to 31 dB relative to the MUSIC sensor noise level.

4.3 Stratus Simulations

Three stratus scenes were simulated in a geometry similar to the MUSIC stratus data. In these cases, the camera was above the clouds looking at them at a grazing angle of 20 degrees. Two cloud layers were used, each one thousand feet thick. By flying the simulated camera at the MUSIC platform speed, decorrelation of successive images due to relative three-dimensional motion of the cloud layers could be examined. As with the cirrus simulations, only the condensed water content parameters were varied, as shown in Table 3.

4.4 Simulation PSD Analysis

Figure 9 shows the results of PSD analysis of the Cirrus sim4 case, performed analogous to the data processing in Section 3. The anisotropy of the PSD slices is quantitatively similar to that of the cirrus MUSIC data. For both cirrus and stratus simulations, Table 3 shows the results of the PSD analysis for the power law roll-off and the clutter anisotropy.

Table 3. Results of PSD Analysis of the Simulated Cirrus and Stratus Scenes

Case	Mean water lapse rate (g/m^3 ° km)	Condensed water variance at cloud bottom	Clutter to noise ratio (using MUSIC noise level) (dB)	Clutter Specturm Azimuth Roll-off Index	Clutter Spectrum Elevation Roll-off Index	Comments
STRATUS SIMULATIONS						
sim1	1.2	3.0	34.7	-4.8	-5.4	optically thick
sim2	0.6	1.2	28.8	-4.7	-5.3	nominal case
sim3	0.04	0.81	14.6	-6.0	-5.0	low fluctuations
CIRRUS SIMULATIONS						
sim1	0.01	1.0	31.1	-6.4	-5.1	optically thin
sim2	1.0	1.0	13.1	-3.6	-2.5	optically thick
sim3	0.1	5.0	20.6	-5.2	-2.6	high fluctuations
sim4	0.1	1.0	11.7	-3.6	-3.0	"nominal case"

For the cirrus simulations, the range of power law indices and clutter to noise ratios (CNR) is similar to the observed ranges in the MUSIC cirrus data. In addition, the degree of anisotropy of the spectra, as gauged by the separation of azimuth and elevation slices of the 2-D PSD, are also similar. Both data and simulation are much less anisotropic than the predictions

of a simple 2-D perspective distortion model.

4.3 Temporal Coherence Model

The coherence between pairs of image frames at various time lags can reveal important information about cloud dynamics, radiative transfer, the IR sensor itself, and processing algorithms, because coherence is a sensitive measure of systematic effects in any of these phenomena. In the past, analysis of the temporal coherence of IRAMMP data showed that it behaved as[1]

$$|\gamma_{IRAMMP}(\vec{k},\Delta t)|^2 \sim \exp\{-k^2 \Delta t\, D\} \quad (\Delta t > 1\,\text{sec}) \quad , \tag{3}$$

where Δt is the lag time and D is some a coefficient analogous to a diffusion parameter. However, the analysis of the MUSIC data, with its much faster frame rate, has shown that for time lags less than one second, the coherence behaves as

$$|\gamma_{MUSIC}(\vec{k},\Delta t)|^2 \sim \exp\{-k^2 \Delta t^2 \sigma_v^2\} \quad (\Delta t < 1\,\text{sec}) \quad , \tag{4}$$

where σ_v^2 represents an effective rms velocity. In order to account for both of these behaviors, we have modeled the expected coherence from an advecting cloud system.

The motion of clouds within a series of frames is described by an effective two-dimensional velocity field $\vec{V}(\vec{x},t)$ at each position $\vec{x}$ in a frame at frame time t. Since we are using the data after registration, the velocity field of interest is the residual field after the gross cloud motions have been removed. Consequently, there is relatively little motion of the clouds on scales larger than the size of the registration patch size. Each frame is modeled as an advective local shift of the first frame by the velocity field:

$$I(\vec{x},t) = I(\vec{X}(\vec{x},t), t = 0) \quad . \tag{5}$$

The advective position satisfies the implicit equation for motion of a particle in a velocity field:

$$\vec{X}(\vec{x},t) = \vec{x} + \int_0^t dt'\, \vec{V}(\vec{X}(\vec{x},t'),t') \quad . \tag{6}$$

The coherence is formed by averaging over the cloud intensity fluctuation and the velocity field realization, which are assumed to be independent of each other and gaussian (although the gaussian velocity assumption can be removed for some of the results below). For a velocity field variance σ_v^2 and normalized correlation function ρ, the coherence function γ becomes

$$\gamma(\vec{k},\Delta t) = \frac{1}{P(\vec{k})} \int \frac{d^2q}{(2\pi)^2} P(\vec{q}) \int d^2y \exp\{i\vec{y}\cdot(\vec{q}-\vec{k})\}$$

$$\times \exp\left\{-\frac{q^2\sigma_v^2}{2}\int_0^{\Delta t} dt_2 \rho(0,t_1-t_2)\right\} \tag{7}$$

$$\times \exp\left\{-q^2\sigma_v^2 \int_0^t dt_1 \int_0^{t+\Delta t} dt_2 \left(\rho(0,t_1-t_2) - \rho(\vec{X}(\vec{x}+\vec{y},t_1) - \vec{X}(\vec{x},t_2), t_1-t_2)\right)\right\}$$

In this result $P(\vec{k})$ is the 2-D PSD of the clutter, and the advected positions are evaluated with the ensemble mean flow field. Typically, registration has reduced the mean flow field to zero. Because registration is performed in order to eliminate the gross

motion of the cloud field, the patches used in the registration procedure are made small enough to minimize motion within a patch. In that case the spatial correlation of the after-registration motion is very high within patch-sized regions, and the last exponential factor in Equation 7 is effectively unity. To lowest order then, the coherence satisfies

$$|\gamma(\vec{k},\Delta t)|^2 = \exp\left\{-k^2\sigma_v^2\int_0^{\Delta t}dt_1\int_0^{\Delta t}dt_2\,\rho(0,t_1-t_2)\right\} \tag{8}$$

From this expression, there are two extreme limits in which we can examine the behavior of the coherence function. The first limit is the small time-lag regime. For time-lags much smaller than the characteristic integral time scale of the correlation function, the correlation is effectively 1, so that in the short time-lag limit, the coherence is

$$|\gamma(\vec{k},\Delta t)|^2 = \exp\left\{-k^2\sigma_v^2\Delta t^2\right\} \tag{9}$$

This is exactly the behavior found empirically in the MUSIC data analysis, and we interpret the effective rms velocity in the MUSIC data is the true two-dimensional rms velocity.

The second limit is for time lags comparable to or larger than the integral time scale T of the velocity fluctuations, defined as

$$T=\int_0^{\infty}dt\,\rho(t) \tag{10}$$

In this case the coherence reduces to an exponential dependence on time analogous to Equation 3, with diffusion coefficient D given by

$$D = \sigma_v^2 T \tag{11}$$

This is the behavior noted previously in the IRAMMP data. Because the IRAMMP sensor has a frame time of approximately 1/2 second, and the MUSIC sensor 1/80 second, the two datasets are complementary tests of this model.

The value of σ_v^2 derived from the MUSIC data analysis is shown in Table 4 for the stratus cases. These values are too high for σ_v^2 to represent an rms velocity intrinsic to the evolving cloud field. Instead, they appear to be due to relative motion of layers of the 3-D cloud. The partial transparency of the foreground portion of the field allows the sensor to also see layers further away. Because of changes in perspective as the camera moves, the farther layers appear to move slower due to their greater range from the camera. When this type of apparent motion is significant, the rms velocity scales with the behavior

$$\sigma_v \approx \frac{\Delta R}{R}\,V_{sensor}\ , \tag{12}$$

where R is the average range to the 3-d cloud, ΔR is the difference in range between the foreground and background cloud layers, and V_{sensor} is the sensor speed relative to the cloud field. Table 4 shows the predicted differential ranges ΔR for the MUSIC data and for the three stratus simulations. As a simple model of perspective-induced decorrelation, and without any truth data about the structure of the clouds, the agreement within a factor of 3-4 seems good.

The results in this section represent the first time high temporal and spatial resolution data have been compared with models in realistic IRST geometries. The model comparisons clearly shown that the cloud clutter exhibits significant three-dimensional behavior in both cirrus and stratus conditions. It would be useful to extend this analysis to cumulus conditions as well.

Table 4. RMS Velocities and Differential Ranges for the MUSIC Data and Stratus Simulations

Case	Range (km)	σ_v (m/s)	ΔR (m)
STRATUS SCENES			
6-2	9.1	11	530
6-3	11.1	23	1300
6-4	20.0	19	1900
6-5	20.0	14	1400
stratus sim1	20.0		480
stratus sim2	20.0		460
stratus sim3	20.0		540
CIRRUS SCENES			
4-1	40.0	20	4900

SECTION 5. CONCLUSIONS

The analysis presented in this paper has provided several new insights about clouds as clutter in IRST problems. The spatial structure of clouds, as measured by the power spectral density, is effectively a power-law with a breakpoint and roll-off that is cloud type and look geometry dependent. For cirrus clouds, the power-law index is about -5 ± 1.5, and for stratus scenes it is about -4.5 ± 0.5. The degree of anisotropy in the PSD at low grazing angles is due to the underlying three dimensional character of the clouds. This conclusion is based on (1) the agreement of power-laws between data and the 3-D simulator; and (2) simple models invoking two-dimensional clouds with parallax-induced anisotrpy predict much larger anisotropy than observed. Clutter to noise levels for both cloud types range from 13 dB to 32 dB, which is seen in the simulator as well. These large CNR levels represent potentially large noise sources for IRST.

The temporal coherence of sequences of MUSIC cloud scenes, after the registration process, has a simple dependence on the square of the spatial frequency and the time delay. This behavior is effectively modeled in terms of passive advection of cloud elements, with a stochastic velocity field that is highly correlated over scales larger than the registration patch size. The model also successfully predicts the behavior of IRAMMP data observed in a previous analysis for larger time lags.

SECTION 6. REFERENCES

1. M. S. Farber, S. J. Hemple, B. A. Eckstein, "Characterization of IRAMMP Data Using Scene Registration," IRIS Proceedings, January 1991.
2. L. E. Hoff and E. M. Winter, "Demonstration of Clutter Reduction and Aircraft Detection in Multispectral Data," SPIE Proceedings, Volume 1698, 1992.
3. Alan D. Stoder et al, "Spectral and Temporal Processing of MUSIC Sensor Data," IRIS Proceedings, January 1992.
4. R. F. Cahalan and J. B. Snyder, "Marine Stratocumulus Structure," Remote Sens. Environ. **28**, 95-107
5. P. F. Hein and S. K. Cox, "Spatial Scales of Cirrus Cloud Properties," Fire Scene Team Proceedings, June 1989.
6. L. Thebaud, et al, "Statistics of IR Cloud Images - A Modeling Approach," Cloud Impacts on DoD Operations and Systems, 1991 Conference (CIDOS - 91), 9-12, July 1991.
7. J. Tessendorf, D. Weston, L. Taylor, "Structure of Spatial Spectra of Simulated Cloud Scenes at Infrared Wavelengths," Characterization, Propagation, and Simulation of Sources and Backgrounds II, SPIE 1687, 499-507, 1992.
8. J. Pendat and A. Piersol, Random Data: Analysis and Measurement Procedures, John Wily and Son, 1971.
9. J. Tessendorf, et al, "Modeling and Simulation of Complex Cloud Scenes at IR Wavelengths," IRIS Proceedings,

January 1992.

ACKNOWLEDGEMENTS

The authors wish to acknowledge the help given by Stuart Hemple in developing some of the basic analysis tools used here, and Justin Kocher for developing the analysis and graphics output. We also wish to thank Evelyn Baker for preparing the manuscript.

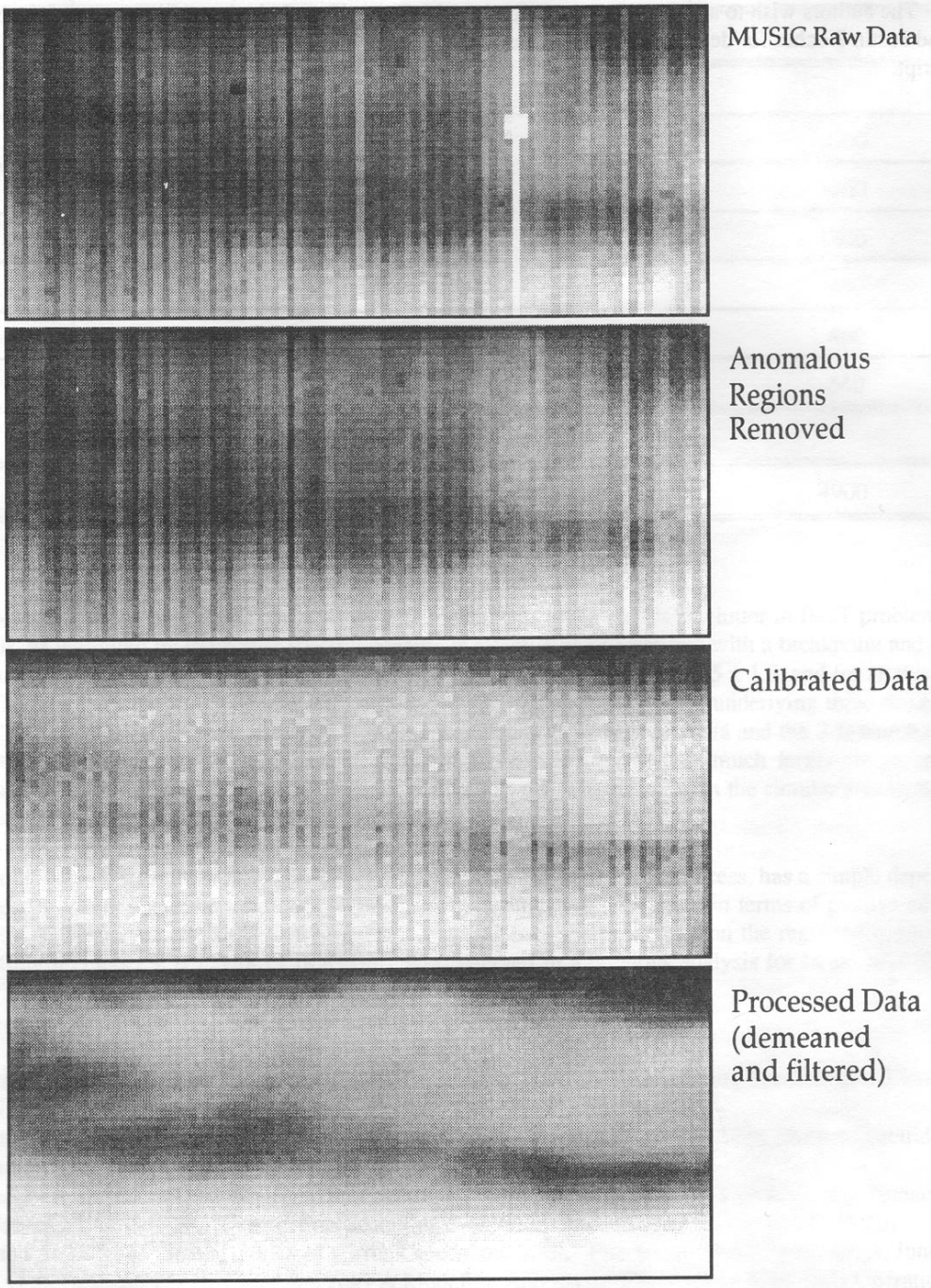

Figure 1. MUSIC Pre-processing on a Cirrus Scene (MUSIC 4-1a shown)

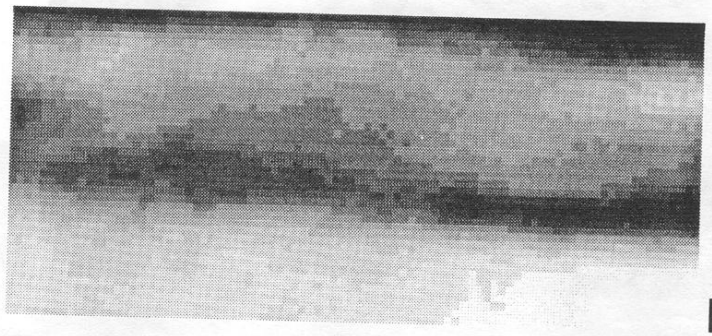

MUSIC 4-1a

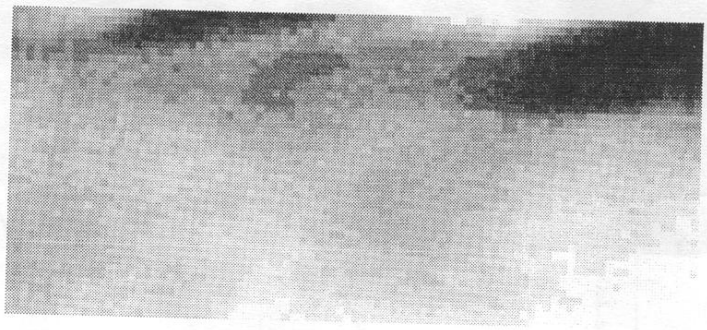

MUSIC 4-2

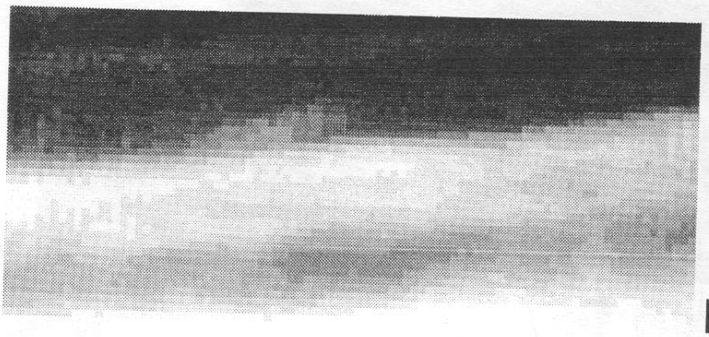

MUSIC 5-2a

MUSIC 5-2b

Figure 2. Selected Cirrus Scenes

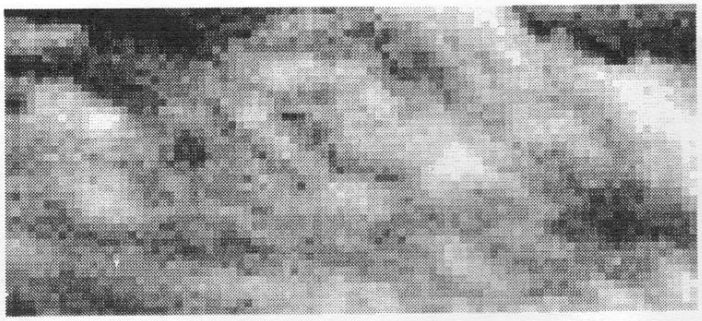

MUSIC 6-3

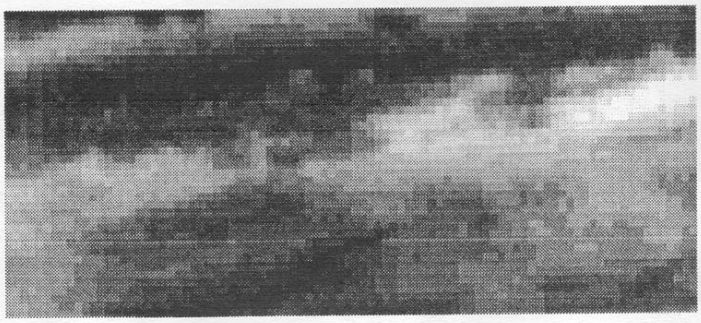

MUSIC 6-4

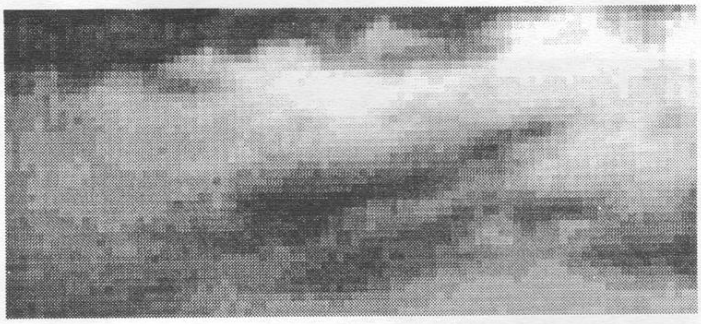

MUSIC 6-5

MUSIC 6-6

Figure 3. Selected Stratus Scenes

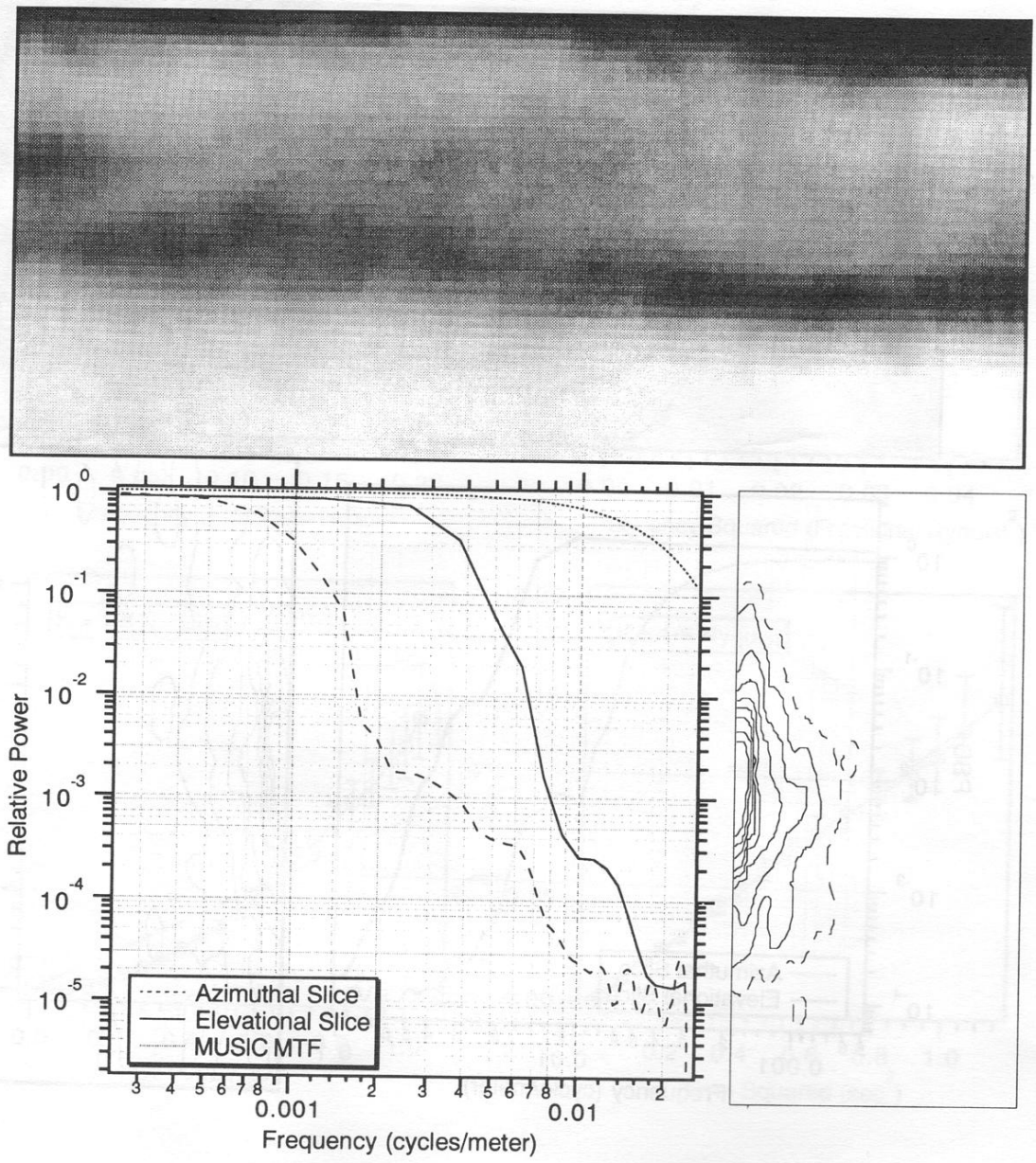

Figure 4. PSD Analysis of a Cirrus Scene (MUSIC 4-1)

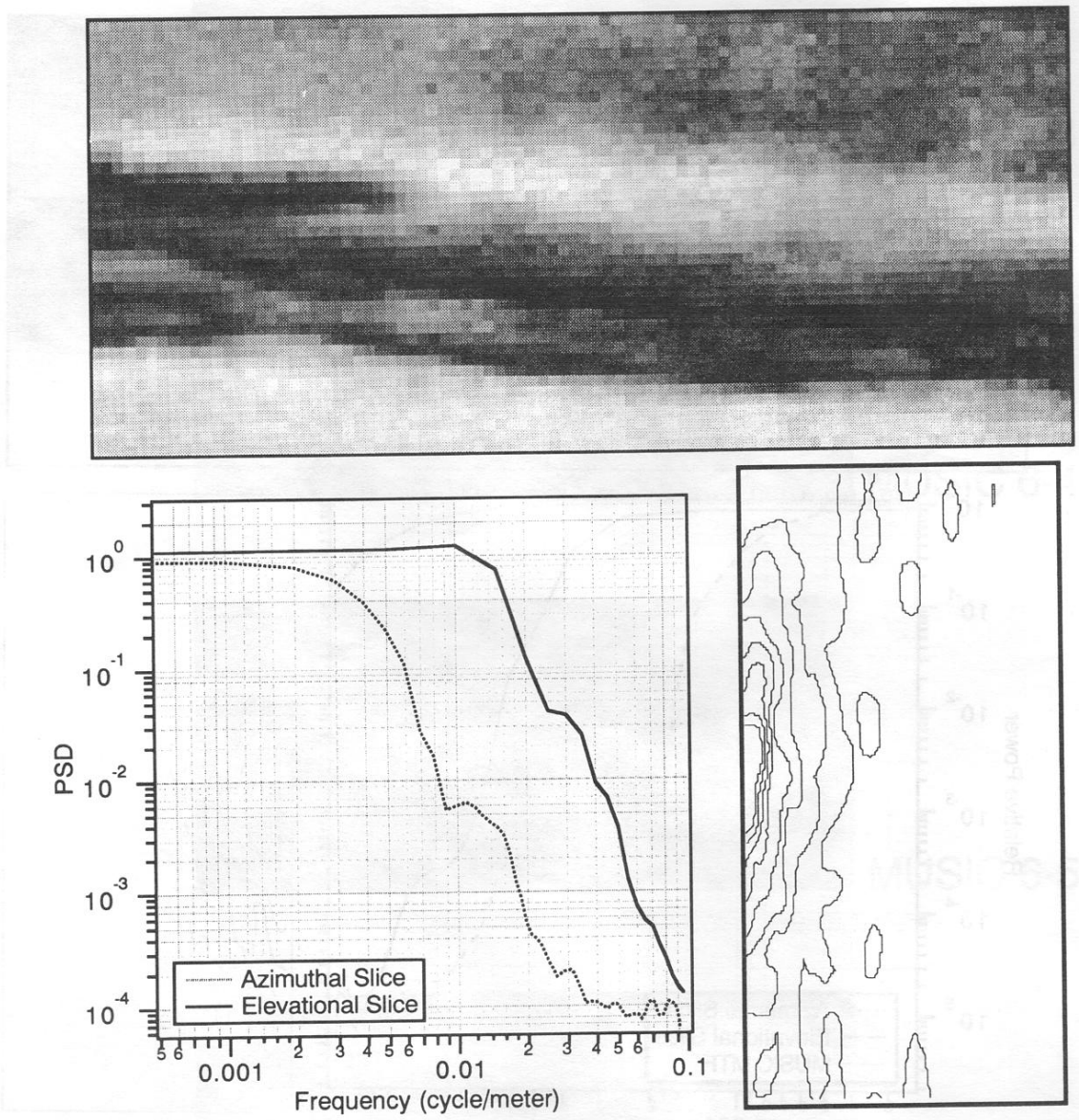

Figure 5. PSD Analysis of a Stratus Scene (MUSIC 6-2)

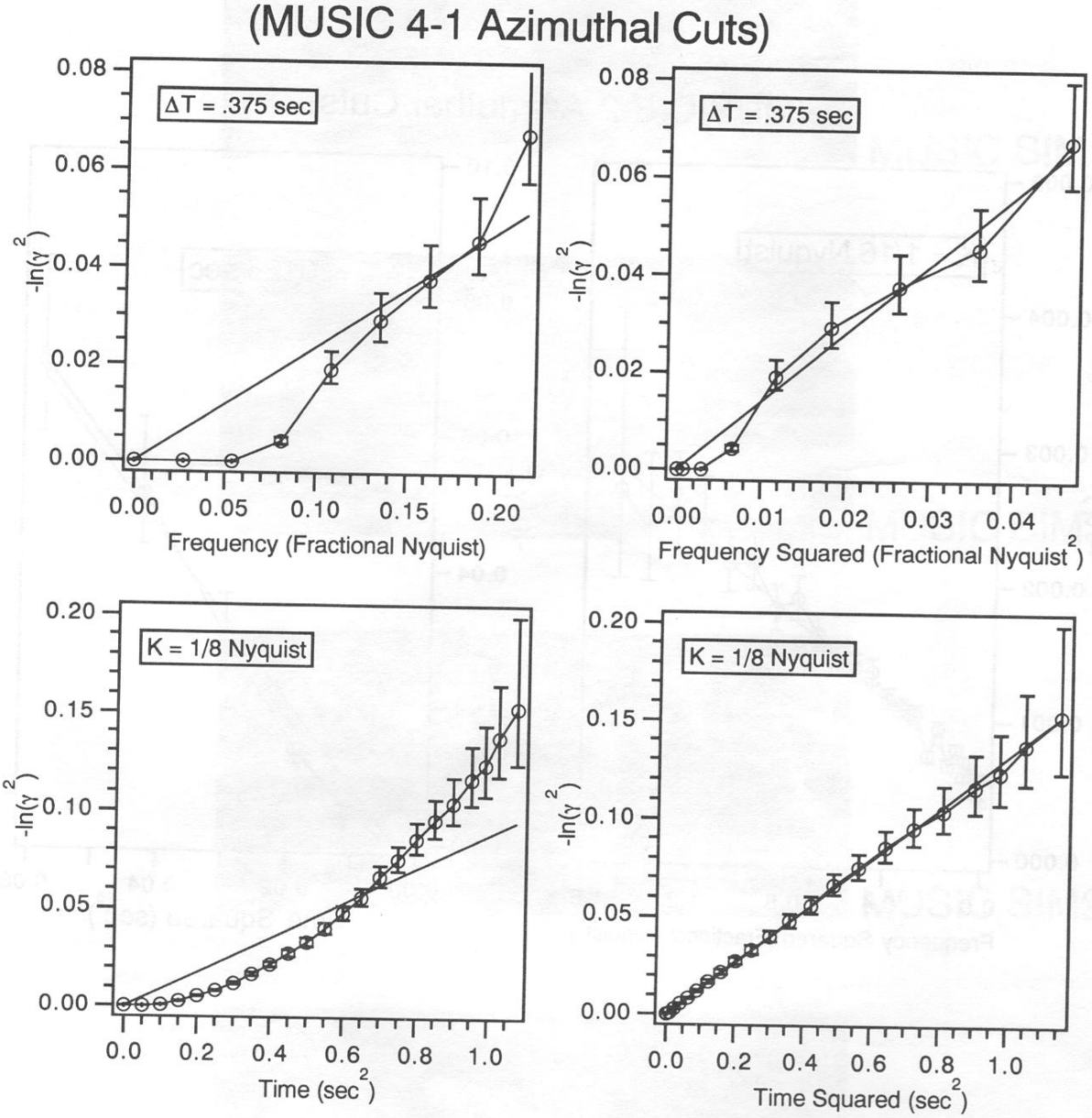

Figure 6. K^2, T^2 Dependence of Coherence Function for a Cirrus Scene (MUSIC 4-1 Azimuthal Cuts)

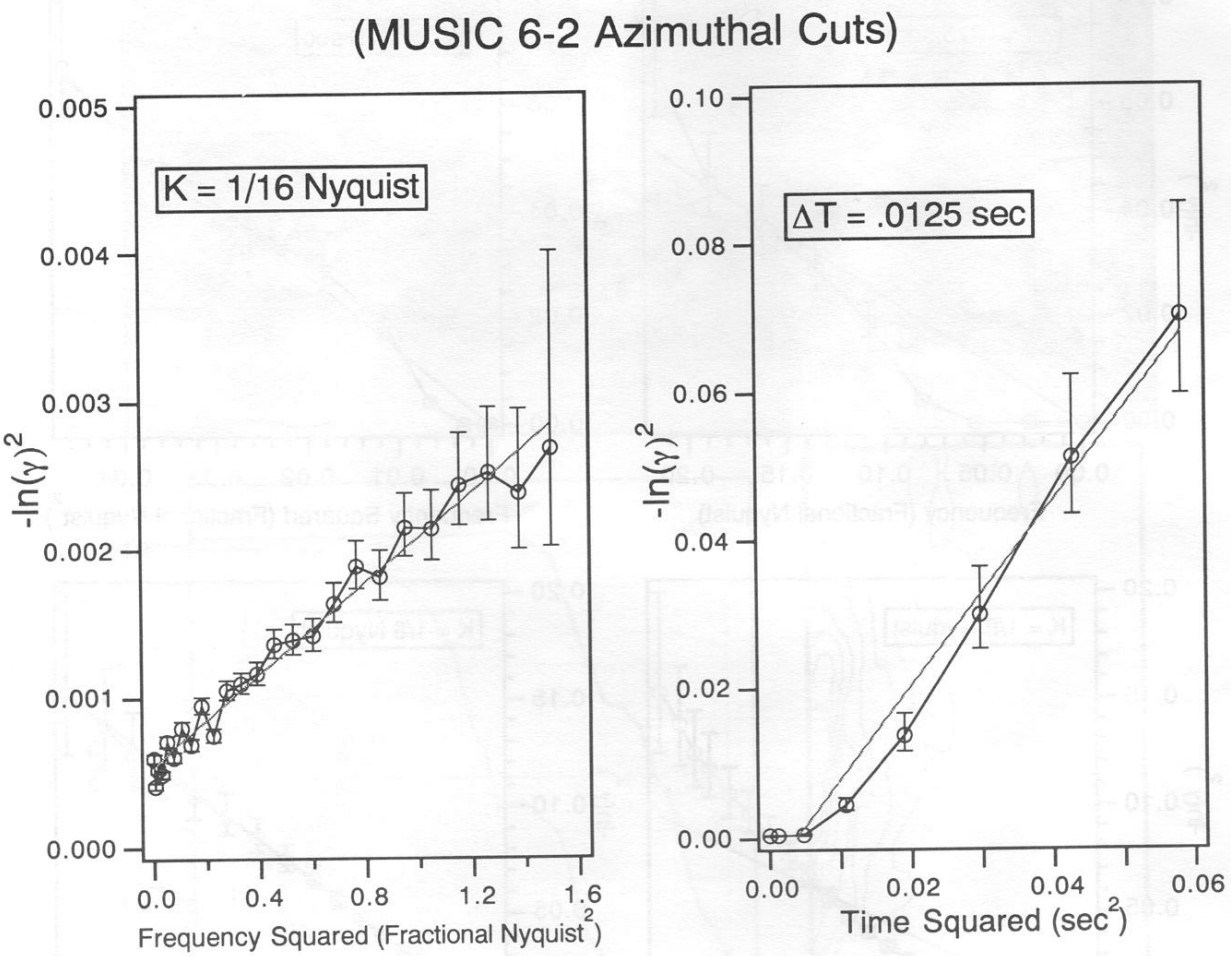

Figure 7. K^2, T^2 Dependence of Coherence Function for a Stratus Scene (MUSIC 6-2 Azimuthal Cuts)

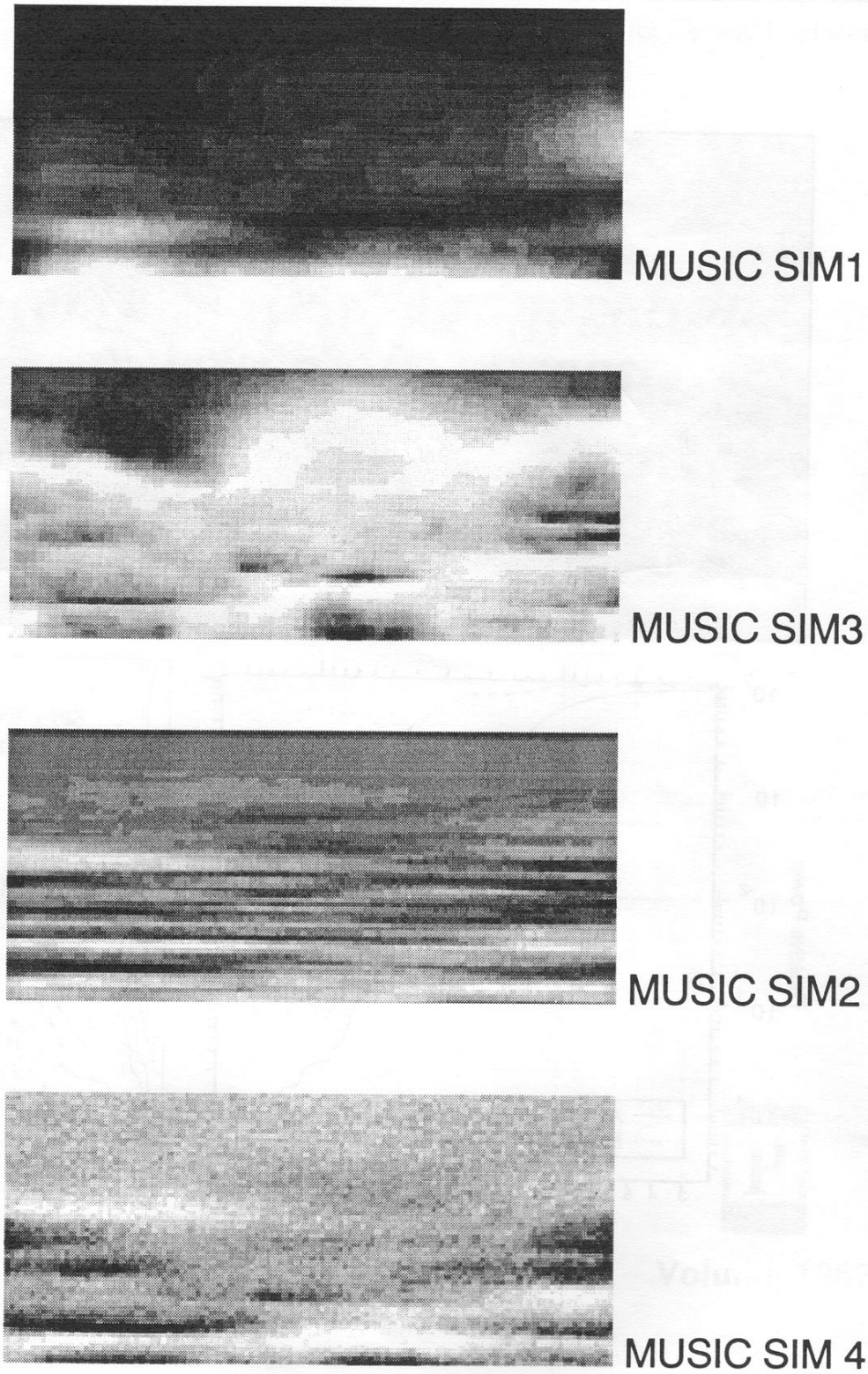

Figure 8. MUSIC Cirrus Simulation Scenes

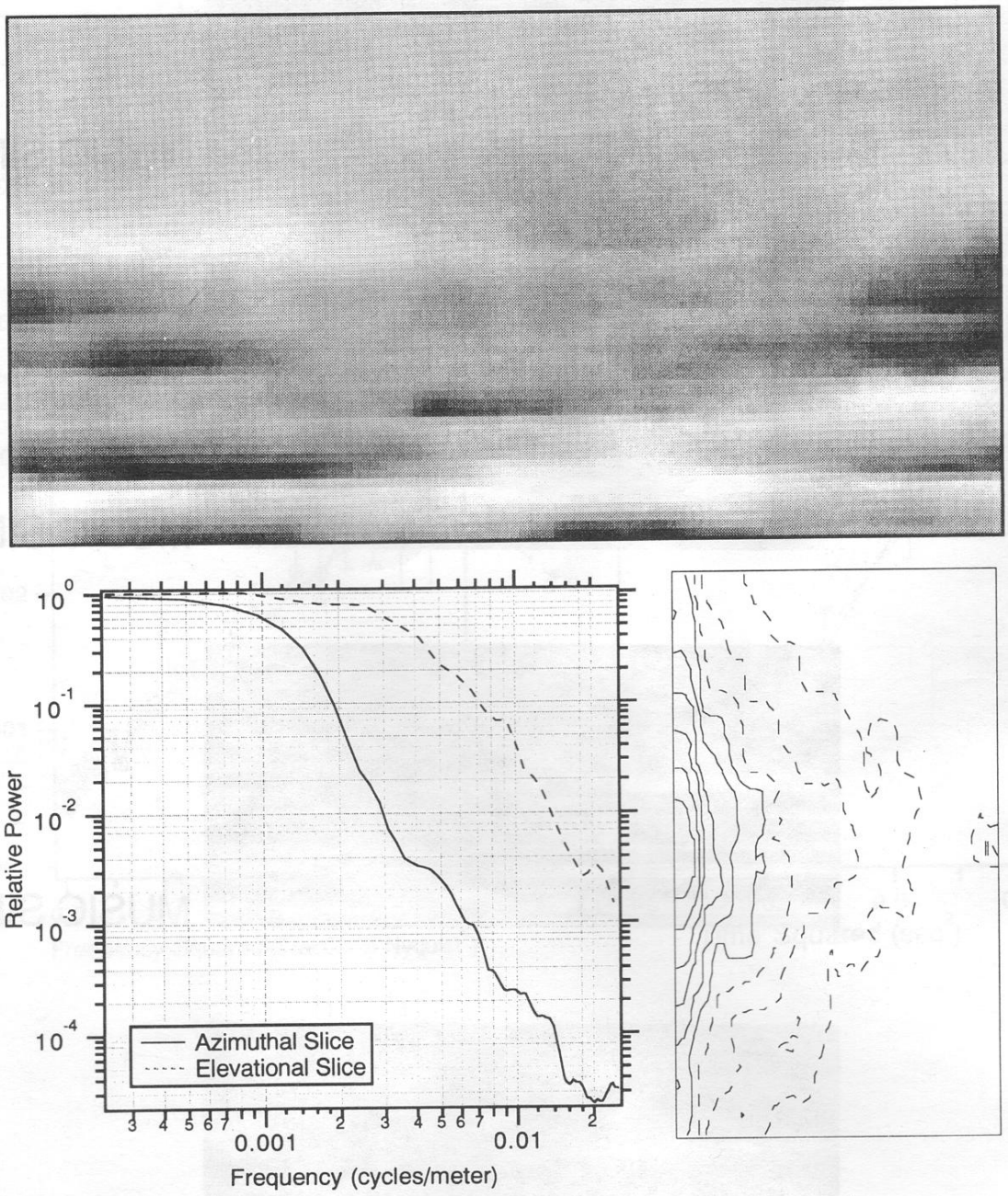

Figure 9. MUSIC Cirrus Simulation Scene PSD Analysis